Materials Research Proceedings 41 (2024) 234-241 https://doi.org/10.21741/9781644903131-26

# On the experimentation of the laser-powder bed fusion process for high-strength aluminum alloys

EL HASSANIN Andrea[1,a *], PERNA Alessia Serena[1,b], SICIGNANO Nicola[1,2,c], BORRELLI Domenico Borrelli[1,2,d], CARAVIELLO Antonio[1,2,e] and ASTARITA Antonello[1,f]

[1]Department of Chemical, Materials and Production Engineering, University of Naples Federico II, Piazzale V. Tecchio 80, 80125 Naples, Italy

[2]Sòphia High Tech S.r.l, Via Malatesta 30 A, 80049, Naples, Italy

[a]andrea.elhassanin@unina.it, [b]alessiaserena.perna@unina.it, [c]nicola.sicignano@sophiahightech.com, [d]domenico.borrelli@sophiahightech.com, [e]antonio.caraviello@sophiahightech.com, [f]antonello.astarita@unina.it

**Keywords:** Laser-Powder Bed Fusion, Aluminum Alloys, Material Characterization

**Abstract.** Additive Manufacturing (AM), a cutting-edge technique developed for the manufacture of prototypes that aims to produce large-scale products tailored for numerous industrial applications, has found increasing space in recent years. In this context, Laser-Powder Bed Fusion (L-PBF) technology represents one of the most intriguing ones considering the large number of processable and under-development alloys. By combining the inherent benefits of this technology, it is then possible to produce components with improved mechanical characteristics and low weight. Nevertheless, improved properties such as thermal and electrical conductivity, strength, and corrosion resistance can be achieved. In this scenario, high-performance aluminum-based alloys, tailored for the metal AM have raised increasing interest in the industrial framework. In this work, the LPBF processing of an Al-Mg-Sc-Zr was investigated. The tensile characteristics, the microhardness, the density and the microstructure of L-PBF specimens were analyzed.

## Introduction

The use of powder-based Additive Manufacturing (AM) technologies is transforming the process of creating tailored parts. In this field, Laser-Powder Bed Fusion (L-PBF) is particularly notable as the most cutting-edge and dependable technique for fabricating metal objects [1,2]. In the past few years, there was a significant amount of investigation into the application of Laser-Powder Bed Fusion (LPBF) technology for the AM of metal parts [3,4]. This research explored the use of various pure metals and alloys, the latter including steel, aluminum, titanium, and nickel alloys [5–7].The primary focus of this research has been two-fold: the creation of complex-shaped parts and the development of materials that possess enhanced mechanical properties and customized physical characteristics to meet the specific requirements of high-performance applications. Among the different types of materials employed in traditional manufacturing techniques, only a limited few have been tailored for additive manufacturing to enhance the manufacturing process. In the most competitive industrial sectors, like the aviation sector, it is imperative to employ a metal alloy with an optimal blend of mechanical properties, including high strength and stiffness but also good formability. Hence, accurately evaluating the underlying metallurgical mechanisms is critical in attaining these desired qualities. In this scenario, the aerospace industry makes extensive use of high-strength Al alloys to create structural components [8]. These alloys offer exceptional strength-to-weight and stiffness-to-weight ratios, which, when coupled with the advantages of AM techniques, result in minimized material wastage and energy usage throughout the fabrication process [9].

As a result, the final aircraft exhibits enhanced fuel efficiency, thus reducing its environmental impact during operation. To address these challenges, researchers are conducting more studies to expand the range of usable alloys and developing methods to detect and rectify the different types of defects that may arise during L-PBF [10]. The focus of this study was to investigate the processability window through L-PBF of an Al-Mg-Sc-Zr alloy. This work studied the effect of the main L-PBF process parameters, namely laser power and scanning speed, on the final processability through L-PBF of the Al-Mg-Sc-Zr alloy, whose mechanical properties are enhanced both through solid dispersion and precipitation hardening [11]. To evaluate the mechanical properties, tensile tests were performed on the printed specimens. The tensile tests provided insights into the strength, ductility, and deformation behavior of the printed alloy. Vickers microhardness measurements were carried out to assess the hardness distribution and variations within the printed specimens. Density measurements were conducted to determine the porosity level in the printed specimens, as porosity can significantly influence the mechanical properties of the alloy. Microstructural analysis was performed using various techniques, such as optical microscopy and SEM-EDS. This analysis aimed to understand the sensitivity of the chosen alloy against variations of L-PBF processing conditions. Overall, this study provided a comprehensive understanding of the potential of L-PBF for printing Al-Mg-Sc-Zr alloys in the as-built condition: despite it is a age-hardenable alloy, knowing the starting point before heat treatment is necessary also to appreciate the mechanical properties improvement due to the treatment itself. The findings could provide insights for the process development of the selected alloy, given its high feasibility for the production of complex shaped parts with end use in fields where low weight and high performance are required.

## Materials and Methods

L-PBF specimens. For the experimental campaign, powders of Al-Mg-Sc-Zr aluminum alloy were used, supplied as custom powders by Metals 4 Printing [12]. To evaluate the actual composition of the powders, SEM-EDS analysis was carried out using the Oxford Instrument Swift ED 3000 Probe microscope coupled with an Hitachi TM3000 SEM, the latter also used to analyze the powders morphology illustrated in Fig. 1. Moreover, according to the ASTM B822 standard, the following particle size distribution was obtained: $D_{10}$ = 10.7 μm; $D_{50}$ = 30.2 μm; $D_{90}$ = 77.9 μm. Concerning the parts to be printed, it was decided to print 18 cubic specimens (2 specimens per set of process parameters) and 18 dog bone specimens with the same parameters, whose placement inside the process chamber followed the scheme illustrated in Fig. 2. The process parameters values were decided in order to investigate three levels of Volumetric Energy Density (VED, see Table 1), obtained through different combinations of laser power and scanning speed: in this way, the experiments enabled to analyze the feasibility of the process as a function of the most used parameters group, i.e. VED, as well as to check how the different “paths” leading to the same VED values affect the processed material [13], according to the data reported in Table 2. The specimens were printed with a Concept Laser Cusing M2 L-PBF machine, equipped with an yttrium laser source with a maximum power of 400 W and a focus diameter of 70 μm. The specimens were all built with an horizontal positioning on the build platform (see Fig. 1) in order to reduce the feedstock amount required. The material was processed through an island scan strategy, as similarly to other works described elsewhere [14].

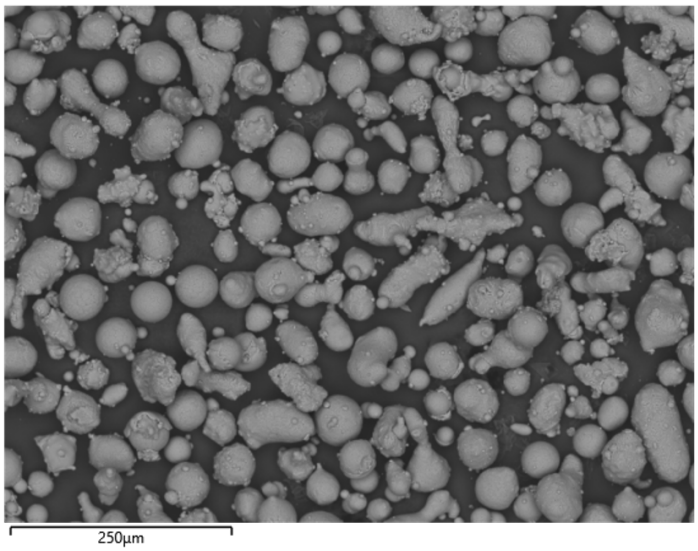


*Fig. 1 – Al-Mg-Sc-Zr powders used in this work.*

*Table 1 – Chemical composition of the Al-Mg-Sc-Zr powder feedstock.*

| **Element** | **Al** | **Mg** | **Sc** | **Zr** |
|---|---|---|---|---|
| **(wt%)** | Bal. | 5.1±0.1 | 0.4 ± 0.1 | 0.7 ± 0.2 |

*Table 2 - Process parameters for printing the test specimens of the experimental campaign.*

| **ID** | **Layer Thickness** *(mm)* | **Laser Power** (W) | **Scan Speed** (mm/s) | **Hatch Distance** (mm) | **VED** ($J/mm^3$) |
|---|---|---|---|---|---|
| ***1*** | 0.03 | 200 | 847 | 0.105 | 75 |
| ***2*** | 0.03 | 200 | 635 | 0.105 | 100 |
| ***3*** | 0.03 | 200 | 508 | 0.105 | 125 |
| ***4*** | 0.03 | 240 | 1016 | 0.105 | 75 |
| ***5*** | 0.03 | 240 | 762 | 0.105 | 100 |
| ***6*** | 0.03 | 240 | 610 | 0.105 | 125 |
| ***7*** | 0.03 | 260 | 1101 | 0.105 | 75 |
| ***8*** | 0.03 | 260 | 825 | 0.105 | 100 |
| ***9*** | 0.03 | 260 | 660 | 0.105 | 125 |

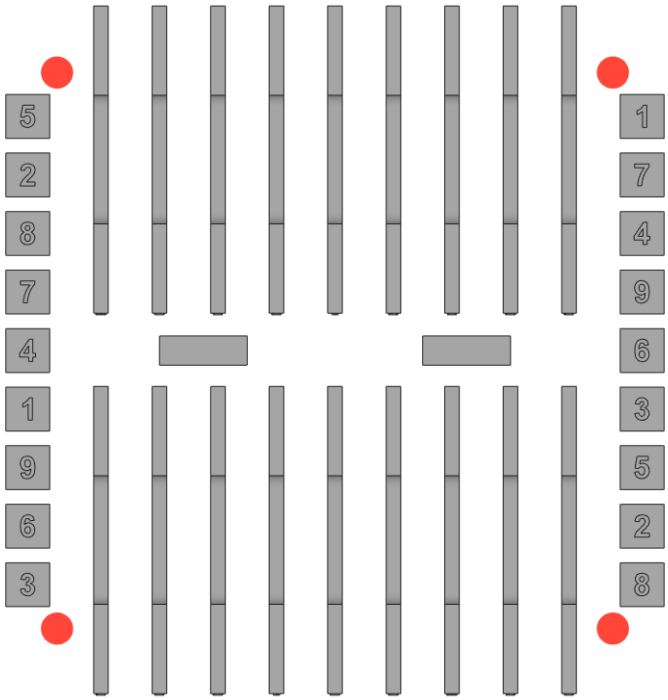


*Fig. 2 – Layout of the L-PBF process for the selected specimens and conditions.*

Characterization procedure. The produced specimens were characterized in terms of density, mechanical properties and microstructure. To this aim, cubic specimens were used for density, Vickers microhardness and microstructure analyses, while dog bone specimens were used for tensile tests. Density measurements were carried out in accordance with ASTM B962 standard, using a Gibertini Eternity 2000 hydrostatic weighing scale after removing the surface roughness of the specimens through grinding. Prior to the Vickers microhardness tests and microstructure analysis, the samples were prepared according to the standard metallographic procedure and polished until the surface quality was 1 μm [15], considering a plane parallel to the build direction of the specimens. The Vickers microhardness was analyzed, in accordance with the ASTM E92-17, through a square-based pyramid indenter with an angle of 148°, performing at least three indentantions on each specimen, with a load of 200g and a dwell time of 15s. Tensile tests were performed according to the ASTM E8M standard and considering the reduced specimen dimensions. The tests were carried out using a Galdabini Quasar 50 universal testing machine, equipped with a 50 kN load cell. Microstructure analysis was carried out after etching the polished specimens with the Keller's reagent by swabbing for at least 30s. Optical microscopy was carried out to take the macrographs of the specimens processed under different conditions at 100x magnification.

**Results and discussion**

Density and mechanical properties. Fig. 3 illustrates the L-PBF specimens produced according to the experimental plan described in the previous section (only 1 replicate is shown). The visual inspection indicated that the specimens were sound and without significant defects. However, tensile specimens exhibited a significant distortion caused by the printing process, considering the remarkable thermal conductivity and thermal expansion coefficient of the selected alloy in combination with the horizontal positioning and the absence of stress relief heat treatment post-build.

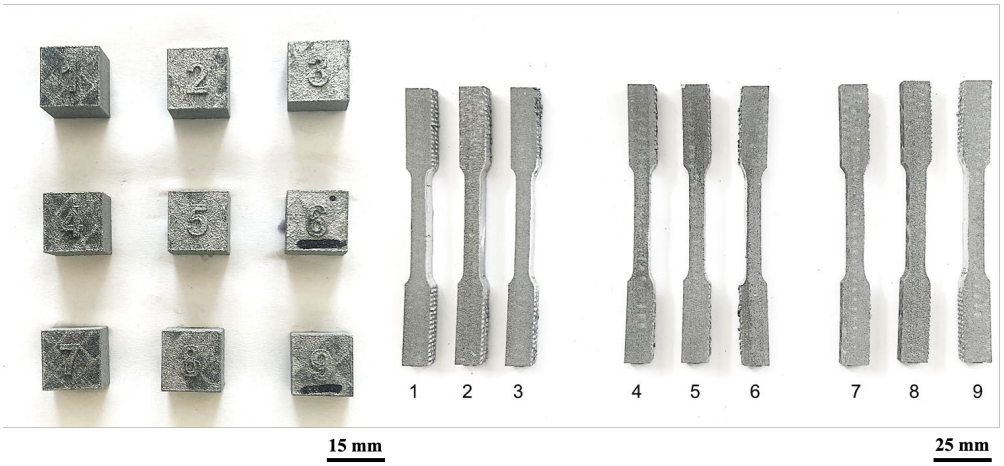


*Fig. 3 – L-PBF specimens produced in this work.*

On the other hand, the relative density measures results, illustrated in Fig. 4, suggested that the selected alloy was quite sensitive against the investigated processing conditions: more specifically, it was found that the highest densities were achieved for the processing conditions related to the lower values of power and scanning speed, regardless of the specific VED value, reaching a maximum value of approximately 97%. This result suggests that the chosen alloy needed a longer interaction time with the laser to enable a consistent melting without a remarkable presence of defects due to lack of fusion [16].

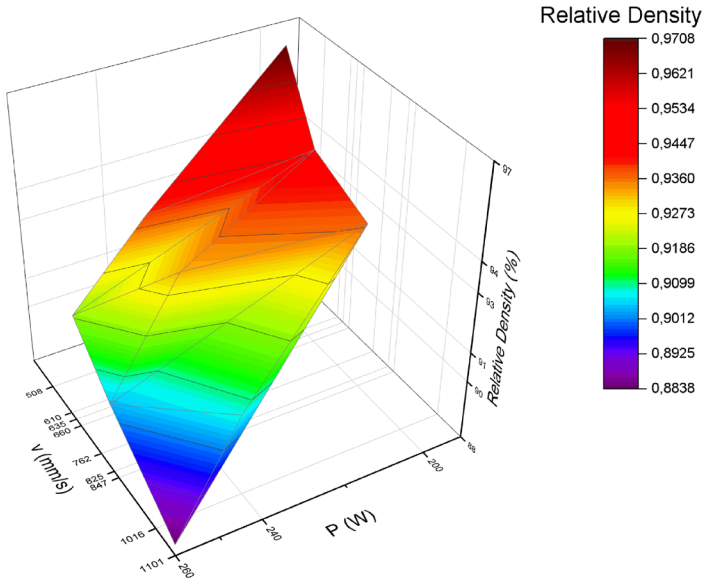


*Fig. 4 – Relative density plot vs varied L-PBF process parameters.*

Concerning the mechanical properties, Table 3 resumes the collected data of Vickers microhardness and tensile properties, reporting for the sake of brevity only the experimental conditions that defined the investigated processing window as well as the central value. Another reason for this choice is that the experimental results were not suggesting remarkable variations for close processing conditions, coherently with the density experimental outcomes. This essay was confirmed also by the results shown in Table 3, that can be synthesized as follows: i) the

microhardness was practically not sensitive to the processing conditions, as the material experienced a steep cooling rate in any case leading to a quenched-like condition after L-PBF; ii) the mechanical strength was affected by the L-PBF conditions, especially in terms of yield strength and elongation at break due to the presence of defects; iii) even if slight variations were observed, the tensile strength and Young's modulus were less sensitive against the L-PBF processing conditions with respect to the other tensile properties.

*Table 3 – Vickers microhardness and mechanical properties of the L-PBF produced specimens that defined the extremes and the middle of the investigated processing window.*

| ID | Vickers microhardness (HV) | Yield strength (MPa) | Tensile strength (MPa) | Elongation at break (%) | Young's modulus (GPa) |
|---|---|---|---|---|---|
| ***1*** | 107±2.9 | 190±20 | 299±30 | 8.8±2 | 69.5±10 |
| ***5*** | 106±4.4 | 241±25 | 291±31 | 18.6±3.3 | 75.4±7 |
| ***9*** | 105±6.2 | 137±18 | 282±45 | 17.2±1.8 | 71.1±9 |

Microstructure and chemical composition. Fig. 5 illustrates the comparison between the cross-sectional views of the specimens ID # 1, 5 and 9 obtained according to the metallographic procedure described in the previous section. The first notable outcome was that the characteristic element that describes the microstructure of the L-PBF processed material, i.e. the molten pool, was not significantly affected in terms of shape as a function of varied processing conditions. This means that the selected processed parameters have not significantly changed the intensity of the laser-powder interaction, leading in any case to molten pools with a with greater than the depth, suggesting therefore the conduction welding mode [17]. Moreover, coherently with the density measurements, the produced specimens presented a notable number of defects, whose irregular shape suggested that the lack of fusion occurred in any case [18]. Despite this latter result, the optical macrographs did not suggest any correlation between the defects observed and the relative density quantified as a function of the process parameters.

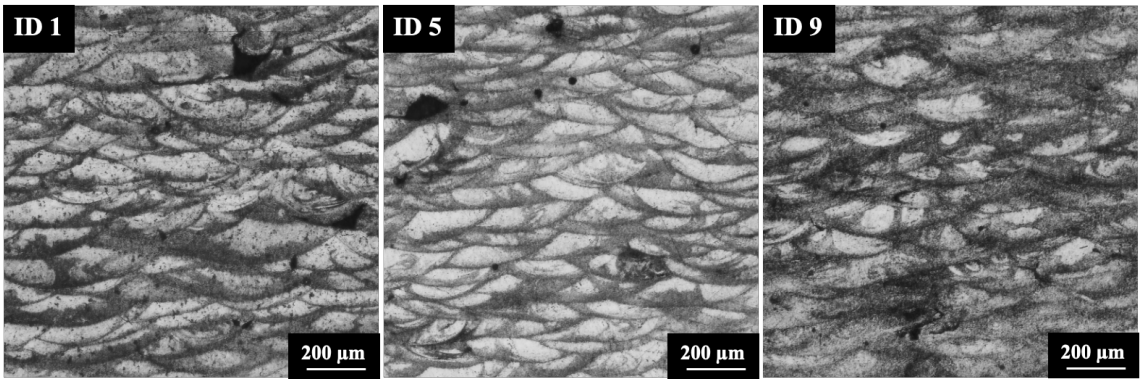


*Fig. 5 – Optical macrographs of the L-PBF specimens that defined the extremes and the middle of the investigated processing window (magnification 100x).*

For what concerns the influence of the selected processing conditions on the chemical composition of the alloy, the EDS results reported in Table 4 highlight that the original was slightly altered by the L-PBF process. However, the reported results could be affected by the specific area considered for the EDS analysis: as the L-PBF process leads to uncontrolled formation and

distribution of intermetallic phases as well as to segregation of elements, it is convincible that these mechanisms make the EDS less robust against the region of interest.

*Table 4 – Chemical composition of the produced L-PBF specimens that defined the extremes and the middle of the investigated processing window.*

| Element (wt%) | Al | Mg | Sc | Zr |
|---|---|---|---|---|
| ***ID 1*** | Bal. | 4.2±0.1 | 0.4 ± 0.1 | 0.4 ± 0.2 |
| ***ID 5*** | Bal. | 4.8±0.1 | 0.4 ± 0.2 | 0.2 ± 0.1 |
| ***ID 9*** | Bal. | 4.1±0.2 | 0.3 ± 0.2 | 0.3 ± 0.2 |

## Conclusions

This work deals with the experimental investigation of the L-PBF processing of an Al-Mg-Sc-Zr alloy, exploring a wide frame of process parameters combination, followed by a characterization of main mechanical and microstructural properties of the parts in the as-built state. The emerged experimental outcomes could be synthesized as follows:

- Every combination of L-PBF processing parameters was feasible for the selected alloy, thus avoiding print interruptions and macroscopic flaws.
- The relative density was highly sensitive to the processing conditions investigated: it was found that higher values, up to approx. 98%, could be achieved when adopting lower laser power and scanning speed values. Vice versa, the lowest relative density of approx. the 88% was measured when the combination of the highest laser power and lowest scan speed was used.
- In general, the Vickers microhardness and the mechanical properties were not particularly affected by the different L-PBF process parameters, except for the yield strength and elongation at break whose values were dependent on the densification of the alloy.
- The microstructure of the processed alloy presented very similar characteristics, including the molten pools shape and the typical lack of fusion defects. The same consideration could be done for the chemical composition, for which a not negligible sensitivity of the EDS techniques might have introduced an uncertainty.

## References

[1] A. Katz-Demyanetz, V. V. Popov, A. Kovalevsky, D. Safranchik, A. Koptyug, Powder-bed additive manufacturing for aerospace application: Techniques, metallic and metal/ceramic composite materials and trends, Manuf Rev (Les Ulis) 6 (2019) 5. https://doi.org/10.1051/mfreview/2019003

[2] W. Abd-Elaziem, S. Elkatatny, A.-E. Abd-Elaziem, M. Khedr, M.A. Abd El-baky, M.A. Hassan, M. Abu-Okail, M. Mohammed, A. Järvenpää, T. Allam, A. Hamada, On the current research progress of metallic materials fabricated by laser powder bed fusion process: a review, Journal of Materials Research and Technology 20 (2022) 681–707. https://doi.org/10.1016/j.jmrt.2022.07.085

[3] A.G. Colomo, D. Wood, F. Martina, S.W. Williams, A comparison framework to support the selection of the best additive manufacturing process for specific aerospace applications, International Journal of Rapid Manufacturing 9 (2020) 194. https://doi.org/10.1504/IJRAPIDM.2020.107736

[4] I. Tolosa, F. Garciandía, F. Zubiri, F. Zapirain, A. Esnaola, Study of mechanical properties of AISI 316 stainless steel processed by "selective laser melting", following different manufacturing strategies, The International Journal of Advanced Manufacturing Technology 51 (2010) 639–647. https://doi.org/10.1007/s00170-010-2631-5

[5] J.L. Leirmo, High Strength Aluminium Alloys in Laser-Based Powder Bed Fusion – a Review, Procedia CIRP 104 (2021) 1747–1752. https://doi.org/10.1016/j.procir.2021.11.294

[6] V.B. Vukkum, R.K. Gupta, Review on corrosion performance of laser powder-bed fusion printed 316L stainless steel: Effect of processing parameters, manufacturing defects, post-processing, feedstock, and microstructure, Mater Des 221 (2022) 110874. https://doi.org/10.1016/j.matdes.2022.110874

[7] T.C. Dzogbewu, D.J. de Beer, Additive manufacturing of NiTi shape memory alloy and its industrial applications, Heliyon 10 (2024) e23369. https://doi.org/10.1016/j.heliyon.2023.e23369

[8] P. Rambabu, N. Eswara Prasad, V. V. Kutumbarao, R.J.H. Wanhill, Aluminium Alloys for Aerospace Applications, in: 2017: pp. 29–52. https://doi.org/10.1007/978-981-10-2134-3_2

[9] M. Javaid, A. Haleem, R.P. Singh, R. Suman, S. Rab, Role of additive manufacturing applications towards environmental sustainability, Advanced Industrial and Engineering Polymer Research 4 (2021) 312–322. https://doi.org/10.1016/j.aiepr.2021.07.005

[10] S.R. Narasimharaju, W. Zeng, T.L. See, Z. Zhu, P. Scott, X. Jiang, S. Lou, A comprehensive review on laser powder bed fusion of steels: Processing, microstructure, defects and control methods, mechanical properties, current challenges and future trends, J Manuf Process 75 (2022) 375–414. https://doi.org/10.1016/j.jmapro.2021.12.033

[11] K.L. Kendig, D.B. Miracle, Strengthening mechanisms of an Al-Mg-Sc-Zr alloy, Acta Mater 50 (2002) 4165–4175. https://doi.org/10.1016/S1359-6454(02)00258-6

[12] Information on https://www.metals4printing.com/home-en/, (n.d.).

[13] A. El Hassanin, A.T. Silvestri, F. Napolitano, D. Borrelli, A. Caraviello, A. Astarita, Investigation of the laser-related parameters in Laser-Powder Bed Fusion of Inconel 718-Cu blends at fixed Volumetric Energy Density, J Manuf Process 99 (2023) 456–468. https://doi.org/10.1016/j.jmapro.2023.05.068

[14] A. El Hassanin, A.T. Silvestri, F. Napolitano, F. Scherillo, A. Caraviello, D. Borrelli, A. Astarita, Laser-powder bed fusion of pre-mixed Inconel718-Cu powders: An experimental study, J Manuf Process 71 (2021) 329–344. https://doi.org/10.1016/j.jmapro.2021.09.028

[15] Kay Geels, Metallographic and Materialographic Specimen Preparation, Light Microscopy, Image Analysis, and Hardness Testing, n.d. https://books.google.it/books?id=oaehZy3Vo1kC

[16] A. du Plessis, Effects of process parameters on porosity in laser powder bed fusion revealed by X-ray tomography, Addit Manuf 30 (2019) 100871. https://doi.org/10.1016/j.addma.2019.100871

[17] T. Ingrassia, V. Nigrelli, V. Ricotta, C. Tartamella, Process parameters influence in additive manufacturing, in: 2017: pp. 261–270. https://doi.org/10.1007/978-3-319-45781-9_27

[18] W. Wang, J. Ning, S.Y. Liang, Prediction of lack-of-fusion porosity in laser powder-bed fusion considering boundary conditions and sensitivity to laser power absorption, The International Journal of Advanced Manufacturing Technology 112 (2021) 61–70. https://doi.org/10.1007/s00170-020-06224-7